

# **Eigenmode-Guided Amplification via Spatiotemporal Active Acoustic Metamaterials**

Wai Chun Wong<sup>1</sup>, Gregory Chaplain<sup>2</sup> and Jensen Li<sup>1\*</sup>

<sup>1</sup>*Centre for Metamaterial Research and Innovation, Department of Engineering,  
University of Exeter, United Kingdom*

<sup>2</sup>*Centre for Metamaterial Research and Innovation, Department of Physics and Astronomy,  
University of Exeter, United Kingdom*

We present a spatiotemporal gain–loss framework for selective acoustic mode amplification illustrated using coupled Helmholtz resonators. In our scheme, the gain or loss in each resonator is determined by the amplitude in adjacent cavities, forming a non-Hermitian yet energy-conserving system. Our scheme enables the system to collapse toward the eigenstate of an effective linear Hamiltonian with the eigenvalue of largest imaginary part, serving as a fixed-point attractor. In dimer systems, we identify exceptional points that separate oscillatory and convergent regimes, allowing controllable switching between mode collapsing and Rabi-type oscillation. By modulating the gain–loss profile over time, we achieve programmable transitions between eigenmodes, with strategically introduced symmetry-breaking perturbations accelerating convergence. Full-wave simulations validate our approach and highlight its potential for acoustic switching, signal processing, and analog computation. Our results establish a new paradigm for sustainable wave control by bridging non-Hermitian physics and time-varying physics in resonant metamaterials.

\* j.li13@exeter.ac.uk

Despite the distinct physical origins and mathematical forms of the wave equations governing electromagnetic, acoustic, and elastic waves, and the need for different types of metamaterials to manipulate them [1-16], universal theoretical frameworks for wave control have emerged across these domains. Notable examples include coordinate transformation for cloaking and illusion effects [17-19], as well as extensions of the constitutive relationship, such as bianisotropy for simultaneous wavefront and impedance control [20,21], and non-Hermitian parameters like gain and loss for managing scattering in disordered media [22-24]. Among these, PT-symmetric wave amplification [25,26] stands out as a compelling form of non-Hermitian control, enabling lasing mode selection [27-29], wave amplifiers [30,31], and enhanced sensors [32,33].

On the other hand, recent advances in time-varying systems allow non-reciprocal propagation, enhanced nonlinearities [34-37], broadband frequency conversion [38], and temporal analogues of spatial interference, such as double-slit diffraction in time [39]. These systems also offer new pathways for wave amplification via parametric mechanisms [40-43]. Combining time modulation and PT-symmetry can thus introduce an immediate application for temporally guided mode amplification or shaping. However, realizing this combination poses key challenges. Passive PT-symmetric systems, relying solely on loss contrast, inevitably lead to energy decay [44], while active systems with gain permit unbounded energy growth until saturation [45], rendering temporal control ineffective or poorly defined. To achieve sustainable and temporally guided amplification, it is beneficial to conserve total energy and reinterpret amplification as a redistribution of energy (with exponentially increasing amplitude ratio) among system modes rather than unchecked growth.

In this work, we propose a spatiotemporal gain-loss potential framework to enable guided mode amplification through the introduction of a cross-site nonlinearity, illustrated using acoustic Helmholtz resonators. The nonlinearity ensures energy conservation, while we show that the system evolves toward the eigenmode of an effective Hamiltonian with an eigenvalue of the largest imaginary part, acting as a fixed-point attractor. In essence, the control is achieved by designing the spatial gain-loss profile to shape the effective Hamiltonian spectrum while the temporal modulation governs the transition dynamics and accelerates convergence. The system can collapse to a fixed eigenmode rather than exhibiting Rabi-like oscillations, as in conventional quantum transitions, with PT-symmetry determining which behavior occurs. Our spatiotemporal approach enables controlled mode amplification with potential applications in selective acoustic filtering, time-varying metamaterials, and analog computation.

We introduce spatiotemporal gain-loss modulation into a dimer system to facilitate guided mode amplification through the following coupled-mode equations:

$$i \frac{d}{dt} \begin{pmatrix} \psi_a \\ \psi_b \end{pmatrix} = H \begin{pmatrix} \psi_a \\ \psi_b \end{pmatrix}, \quad (1)$$

with the nonlinear Hamiltonian

$$H = \frac{1}{2} \begin{pmatrix} \kappa/2 + ig|\psi_b|^2/E & -\kappa/2 \\ -\kappa/2 & \kappa/2 - ig|\psi_a|^2/E \end{pmatrix} \quad (2)$$

where  $\psi_a, \psi_b$  are the complex fields of mode  $a$  and mode  $b$ ,  $\kappa$  denotes the coupling coefficient and  $g$  is the cross-site gain and loss parameter. For  $g > 0$ , the system introduces gain  $\propto |\psi_b|^2$  for mode  $a$  and loss  $\propto |\psi_a|^2$  for mode  $b$ . Although these gain and loss terms make the system non-Hermitian, their specific form ensures the total energy  $E = |\psi_a|^2 + |\psi_b|^2$  is constant of motion, providing sustainable control. The normalization by  $E$  in Eq. (2) also ensures our system is invariant under scaling.

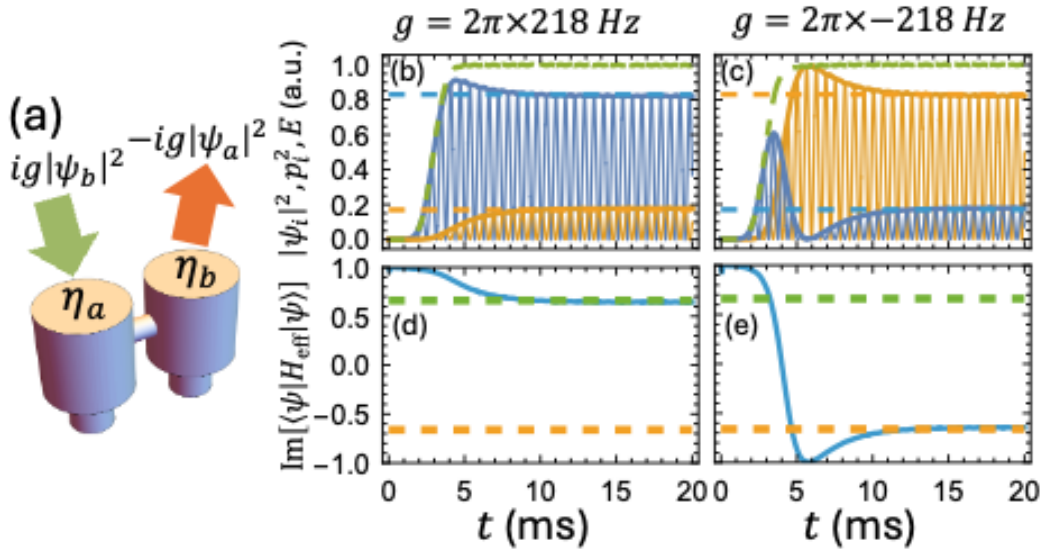


Figure 1 (a) Schematic of acoustics nonlinear dimer in Eq. (1) using two Helmholtz resonators. In 2D FEM simulations, cavity dimensions are width  $w_c = 6$  cm, height  $h_c = 3$  cm, neck dimensions are width  $w_n = 0.5$  cm and length  $l_n = 1$  cm, and bridge dimensions are width  $w_b = 0.2$  cm and length  $l_b = 5$  cm, with identical third-dimension lengths. In simulation, gain and loss  $g$  are introduced via inverted acoustic impedances  $\eta_{a,b}^{-1}$  of the upper wall (e.g.  $\text{Re}(\eta_a^{-1}) \propto g|\psi_b|^2$ ). (b,c) Simulated squared wave amplitudes  $|\psi_a|^2$  (thick blue),  $|\psi_b|^2$  (thick yellow), squared pressures  $p_a^2$  (thin blue),  $p_b^2$  (thin yellow) and total energy  $E = |\psi_a|^2 + |\psi_b|^2$  (green dashed) for (b)  $g = 2\pi \times 218$  Hz and (c)  $g = 2\pi \times -218$  Hz. Dashed horizontal lines show fixed points predicted by  $H_{\text{eff}}$  in Eq. (3). (d, e) Projection metric  $\text{Im}[\langle \psi | H_{\text{eff}} | \psi \rangle]$  of the simulated field state  $(\psi_a, \psi_b)$  (Solid) and eigenvectors of  $H_{\text{eff}}$  (dashed), confirming convergence to the  $H_{\text{eff}}$  eigenvector.

While the nonlinear gain-loss dimer framework applies universally across wave systems, we implement it using coupled Helmholtz resonators, as shown in Fig. 1(a). Here, we interpret  $\psi_{a,b}$  as complex envelopes of pressure in resonators  $a$  and  $b$ , extracted via  $\psi_{a,b} = e^{i\omega t}(p_{a,b} + i\mathbb{H}[p_{a,b}])$ ,

where  $p_{a,b}$  is the physical pressure, and  $\mathbb{H}$  denotes the Hilbert transform, approximated as  $\mathbb{H}[p_{a,b}] \approx \omega \int p_{a,b} dt$ , providing the quadrature component. The  $\omega$  here denotes the carrier frequency which is chosen as the natural resonance frequency of the cavities. Inter-resonator coupling  $\kappa$  arises from the connecting bridge, while the cross-site gain-loss modulation is modeled through time-varying acoustic impedances  $\eta_{a,b}^{-1}$  at the upper cavity walls, with  $\text{Re}(\eta_{a,b}^{-1}) \propto \pm g |\psi_{b,a}|^2$ . In practice, such gain and loss can be realized using feedback loops with microphones and speakers on the cavity walls [46,47]. We investigate the dynamics of the acoustic system using 2D finite-element simulations (COMSOL Multiphysics), assuming invariance along the remaining spatial dimension with parameters specified in the caption of Fig. 1

We validate our spatiotemporal gain-loss framework through mode selection with constant parameter  $g = \pm 2\pi \times 218$  Hz and coupling  $\kappa = 2\pi \times 163$ . Fig. 1(b,c) displays the system dynamics: physical pressure fields  $p_{a,b}^2$  (thin curves) and complex amplitudes  $|\psi_{a,b}|^2$  (thick curves) for resonators  $a$  (blue) and  $b$  (yellow). Within 5 ms, energy is being pumped into the system through the neck of resonator  $a$  while the system converges to distinct attractor states—positive  $g$  concentrates energy in resonator  $a$ , while negative  $g$  favors resonator  $b$ . Total energy  $E = |\psi_a|^2 + |\psi_b|^2$  (green dashed curves) remains invariant after the transient energy pumping period, demonstrating how cross-site nonlinearity enables sustainable amplification without the exponential instabilities of conventional gain systems.

To identify the convergent mode, we introduce a linear effective Hamiltonian capturing the essential physics:

$$H_{\text{eff}} = \frac{1}{2} \begin{pmatrix} \kappa/2 + ig/2 & -\kappa/2 \\ -\kappa/2 & \kappa/2 - ig/2 \end{pmatrix}. \quad (3)$$

This connects to the nonlinear Hamiltonian in Eq. (2) through  $H = H_{\text{eff}} + G I_2$ , where  $G = -\frac{ig}{4E}(|\psi_a|^2 - |\psi_b|^2)$  is a nonlinear common gain-loss term and  $I_2$  is the  $2 \times 2$  identity matrix. Importantly, the system evolves toward the dominant eigenmode of  $H_{\text{eff}}$  for which the eigenvalue has the largest imaginary part, acting as a fixed-point attractor. For our parameters, this yields the dominant eigenmodes  $\psi_+ \triangleq \{0.91, 0.41i\}$  for  $g = 2\pi \times 218$  and  $\psi_- \triangleq \{0.41i, 0.91\}$  for  $g = -2\pi \times 218$ . Following initial transients ( $\sim 5$  ms), the system converges to steady-state intensities, corresponding to steady-state intensities  $\{|\psi_a|^2, |\psi_b|^2\} = \{0.83, 0.17\}$  and  $\{0.17, 0.83\}$  shown as horizontal dashed lines in Fig. 1(b,c). The simulated field intensities (thick curves) precisely match these theoretical predictions after the transient period, supporting the eigenmode collapse mechanism.

To further validate this collapse, we track the projection metric  $\text{Im}[\langle\psi|H_{\text{eff}}|\psi\rangle]$  during evolution. In Fig. 1(d,e), dashed lines represent this metric for the two eigenmodes of  $H_{\text{eff}}$ , while solid curves show this metric for the simulated state  $\{\psi_a, \psi_b\}$ . The simulated state converges precisely to the eigenmode with largest imaginary eigenvalue (upper band for  $g > 0$ , lower band for  $g < 0$ ), confirming that our nonlinear system collapses to the predicted attractor.

Having demonstrated eigenmode shaping through spatial gain-loss distribution, we now exploit temporal modulation to enable dynamic mode switching. Temporal modulation between  $g = \pm g_0$  (where  $g_0 = 2\pi \times 218$  Hz) as illustrated in Fig. 2(a), allows active steering between attractor eigenmodes. The system responds predictably: field intensities  $|\psi_{a,b}|^2$  (solid lines in Fig. 2(c)) converge to  $\psi_+$  for  $g = g_0$  and switch to  $\psi_-$  for  $g = -g_0$ . This temporal control enables on-demand eigenmode selection, with the spatial gain-loss profile determining the available attractors and the temporal modulation selecting between them in real time.

Interestingly in the current dimer case, not all parameter regimes support mode convergence. For reduced modulation depth  $g_0 = 2\pi \times 91$  Hz, the field intensities  $|\psi_{a,b}|^2$  (dashed curves in Fig. 2(c)) exhibit persistent oscillations rather than collapse to a fixed eigenmode. This distinct behavior arises from the PT-symmetry of the effective Hamiltonian  $H_{\text{eff}}$ . In the PT-symmetric phase where  $|g_0| < \kappa$ , all eigenvalues remain purely real (Fig. 2(b)). Without eigenvalue asymmetry in imaginary parts, neither eigenmode dominates as an attractor. Resulting in Rabi-like oscillations, this PT-symmetry transition therefore dictates whether our system exhibits eigenmode collapse (in PT-broken phase) or oscillatory dynamics (in PT-symmetric phase), establishing a fundamental criterion for spatiotemporal mode control.

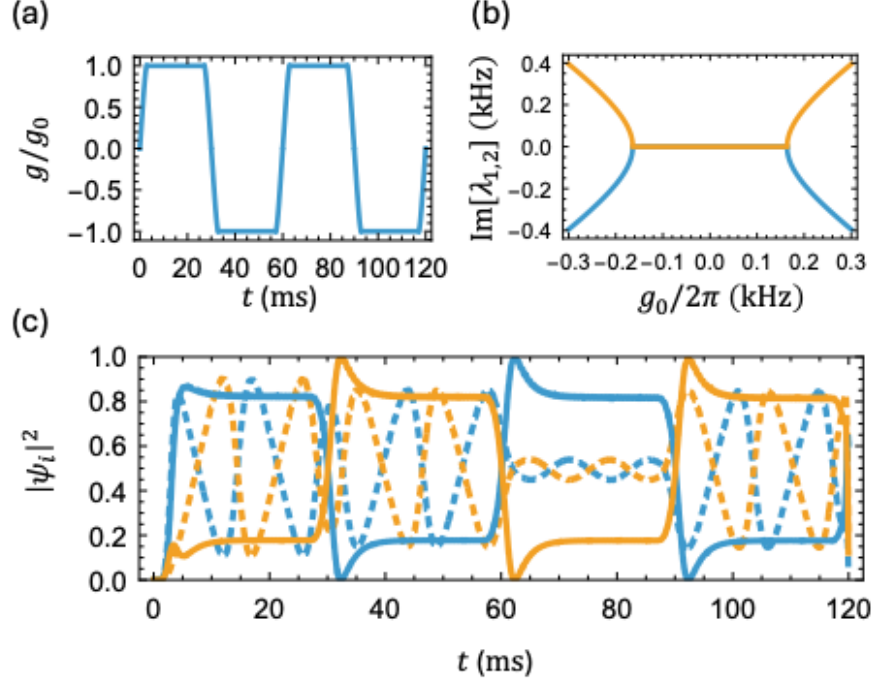


Figure 2 (a) Modulation of the gain-loss parameter  $g$  for dynamic energy switching. (b) The imaginary part of eigenvalues  $\text{Im}[\lambda_{1,2}]$  of the effective Hamiltonian  $H_{\text{eff}}$ . The system exhibits exceptional points (EPs) at gain-loss parameter  $|g_0| = \kappa = 2\pi \times 163$  Hz: for  $|g_0| > \kappa = 2\pi \times 163$  Hz, the system is in the PT-broken phase; for  $|g_0| < \kappa$ , it is in the PT-symmetric phase. (c) Squared field amplitudes  $|\psi_i|^2$  under gain-loss modulation from (a) for  $g_0 = 2\pi \times 218$  Hz (solid, broken phase) and  $g_0 = 2\pi \times 91$  Hz (dashed line, symmetric phase). In the broken phase, the system converges to fixed-point solutions (same as Fig. 1), while in the symmetric phase, it exhibits oscillations without converging to any fixed point.

To understand why the system selects specific eigenmodes, we analyze dynamics in the eigenbasis of  $H_{\text{eff}}$  as  $(\psi_a, \psi_b) = a_1\psi_1 + a_2\psi_2$ , where  $\psi_1, \psi_2$  are eigenvectors with eigenvalues  $\lambda_1, \lambda_2$  (with  $\text{Im}[\lambda_1] \geq \text{Im}[\lambda_2]$ ), we can then derive a key relationship from Eq. (1):

$$\frac{d}{dt} \ln \left( \frac{a_1}{a_2} \right) = -i(\lambda_1 - \lambda_2). \quad (4)$$

This reveals that the amplitude ratio between the two eigenmodes evolves as  $a_1/a_2 \propto e^{-i(\lambda_1 - \lambda_2)t}$ . In PT-broken phase,  $\text{Im}[\lambda_1 - \lambda_2] > 0$  this ratio grows exponentially, causing mode  $\psi_1$  to dominate while  $\psi_2$  vanishes. Conversely, in the PT-symmetric phase ( $|g_0| < \kappa$ ), all eigenvalues are real, yielding  $\text{Im}[\lambda_1 - \lambda_2] = 0$ . Without preferential amplification, the system exhibits persistent oscillations between eigenmodes. We should note that the effective Hamiltonian  $H_{\text{eff}}$  goes beyond conventional Jacobian (stability) analysis by capturing global convergence properties rather than local stability. While Jacobian methods require identifying fixed points before assessing their stability,  $H_{\text{eff}}$

directly reveals the attractor eigenmode through its spectrum, enabling the predictive framework demonstrated above.

We now extend our analysis to three coupled cavities to demonstrate sequential energy routing among multiple targets. For three identical cavities with identical bridges, the dynamics become:

$$i \frac{d}{dt} \begin{pmatrix} \psi_a \\ \psi_b \\ \psi_c \end{pmatrix} = H \begin{pmatrix} \psi_a \\ \psi_b \\ \psi_c \end{pmatrix}. \quad (5)$$

Again, the Hamiltonian can be decomposed into two parts  $H = H_3 + H_{NL}$ , where  $H_3$  is the Hermitian part:

$$H_3 = \frac{1}{2} \begin{pmatrix} \kappa & -\kappa/2 & -\kappa/2 \\ -\kappa/2 & \kappa & -\kappa/2 \\ -\kappa/2 & -\kappa/2 & \kappa \end{pmatrix} \quad (6)$$

and the nonlinear non-Hermitian part is  $H_{NL} = \text{diag}(g_{ab}|\psi_b|^2 + g_{ac}|\psi_c|^2, g_{bc}|\psi_c|^2 + g_{ba}|\psi_a|^2, g_{ca}|\psi_a|^2 + g_{cb}|\psi_b|^2) \frac{i}{2E}$  where initial energy is  $E = |\psi_a|^2 + |\psi_b|^2 + |\psi_c|^2$  and cross-site gain-loss parameters  $g_{ij} = g_i - g_j$ . The parameters  $g_i$  control the relative gain for cavity  $i \in \{a, b, c\}$  among all cavities while conserving total energy. Following the dimer approach, we introduce an effective Hamiltonian:

$$H_{\text{eff}} = H_3 + \frac{i}{6} \begin{pmatrix} g_{ab} + g_{ac} & 0 & 0 \\ 0 & g_{bc} + g_{ba} & 0 \\ 0 & 0 & g_{ca} + g_{cb} \end{pmatrix} \quad (7)$$

where the full Hamiltonian separates as  $H = H_{\text{eff}} + G_3 I_3$  where  $G_3 \propto g_a|\psi_a|^2 + g_b|\psi_b|^2 + g_c|\psi_c|^2 - E(g_a + g_b + g_c)/3$  is a common nonlinear gain term. Despite the increased complexity, the eigenmode dynamics remain analogous to the dimer case: the amplitude ratio  $a_i/a_j \propto e^{-i(\lambda_i - \lambda_j)t}$  for any two eigenmodes  $i, j$ . Therefore, the eigenmode with the largest imaginary eigenvalue will dominate, provided its initial amplitude is non-zero. The mode collapsing behavior settles on a spatiotemporal control of the three cavity gain-loss parameters  $g_a, g_b, g_c$ .

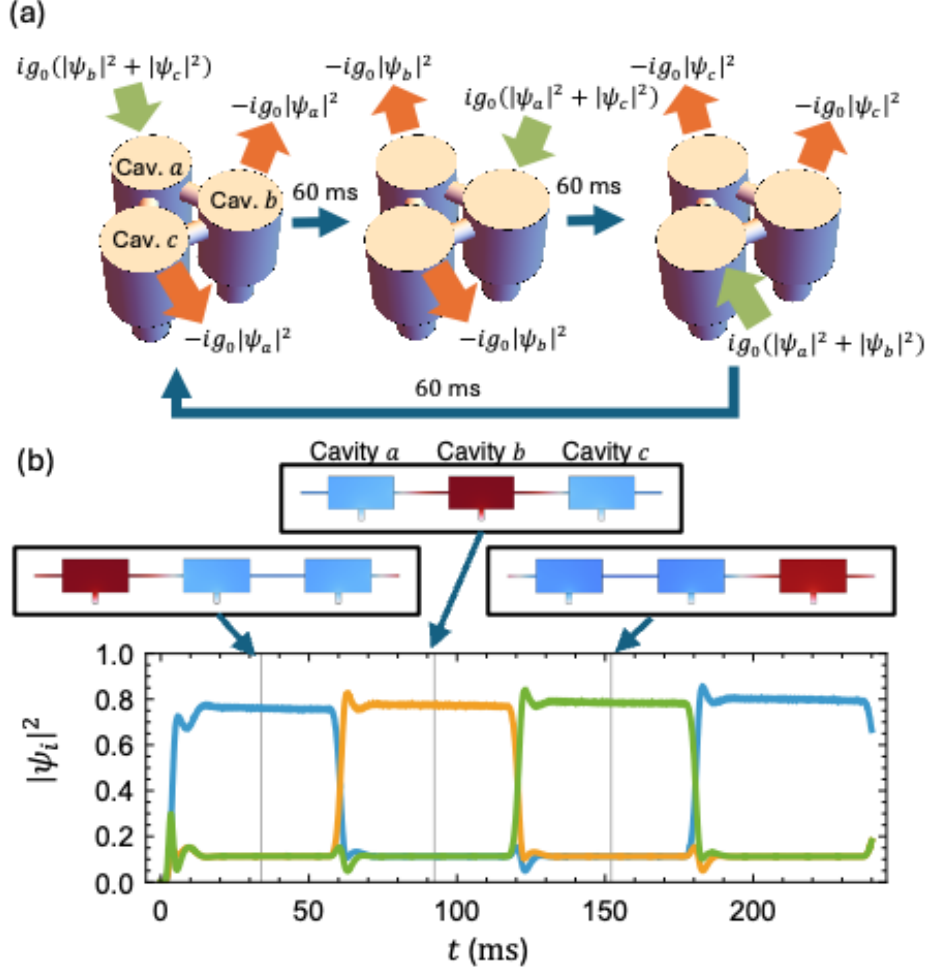


Figure 3 (a) Schematic of energy routing in a nonlinear acoustic trimer with three coupled Helmholtz resonators described by Eq. (5). The cyclic modulation applies relative gain  $g_0$  to each cavity sequentially for 60-ms intervals, i.e.  $(g_a, g_b, g_c) = (g_0, 0, 0) \rightarrow (0, g_0, 0) \rightarrow (0, 0, g_0) \rightarrow \dots$ , implementing energy routing that directs energy sequentially to cavity  $a \rightarrow b \rightarrow c \rightarrow \dots$ . (b) Simulated squared wave amplitudes  $|\psi_i|^2$  for  $i = \{a, b, c\}$  (blue, orange and green). The system converges to different fixed points in each interval, with the gain cavity exhibiting the highest amplitude. Pressure field patterns are shown for each interval.

Now, we demonstrate the spatiotemporal control framework extended to multi-cavity systems, first on a programmed energy routing through cyclic modulation. Figure 3(a) shows temporal control of gain-loss parameters implementing the sequence  $a \rightarrow b \rightarrow c \rightarrow a$  with 60 ms switching intervals. During each interval, a single resonator receives gain ( $g_i = g_0$ , green arrows) while the remaining cavities are balanced ( $g_j = g_k = 0$ , orange arrows). This spatiotemporal modulation creates a time-varying attractor landscape where the dominant eigenmode shifts sequentially between resonators, directing energy flow along the predetermined path.

The full-wave simulated field intensities  $|\psi_{a,b,c}|^2$  in Fig. 3(b) confirm precise sequential routing:



energy concentrates in resonator  $a$  (0-60 ms), transfers to  $b$  (60-120 ms), then  $c$  (120-180 ms), before returning to  $a$ . Using the same gain-loss modulation depth as in dimer case ( $g_0 = 2\pi \times 218$  Hz,  $\kappa = 2\pi \times 163$  Hz), each pumped resonator converges to its corresponding attractor eigenmode. For instance,  $(g_a, g_b, g_c) = (g_0, 0, 0)$  yields eigenmode  $\psi_1 = \{-1.47 - 2.03i, 1, 1\}$  from Eq. (7), with resonator  $a$  achieving maximum amplification. This controlled eigenmode switching enables robust cyclic energy transfer through deliberate spatiotemporal programming.

In fact, the current trimer configuration eliminates the oscillatory regimes found in dimers. Fig. 4(a) shows that eigenvalue spectra maintain clear imaginary part separation. Unlike the dimer's PT-symmetric phase, the eigenmode localizing at the pumped resonator is always the unique dominant eigenmode, ensuring convergence even at low gain. This spectrum enables arbitrary routing sequences without threshold requirements, unlike the dimer case. Recapturing the phase-transition requires us to consider non-identical resonators/coupling with the above eigenmode collapsing mechanism still valid through straight-forward extension.

As another example in tailor-making the eigenmodes to collapse which do not necessarily dominated in a single resonator, we design a spatiotemporal gain-loss profile that transitions from previous single-cavity amplification  $(g_a, g_b, g_c) = (g_0, 0, 0)$  to dual-cavity configuration  $(g_a, g_b, g_c) = (0, g_0, g_0)$  aiming to redistribute energy from resonator  $a$  into equal amplitudes at  $b$  and  $c$  as shown in Fig. 4(b). The target eigenmode  $\psi'_1 = \{0, 1, -1\}$  (with largest imaginary part for eigenvalue) should completely suppress  $a$  while splitting energy between the remaining cavities.

The full-wave simulation results are shown in Fig. 4(c), revealing an unexpected feature in the temporal evolution of field intensities  $|\psi_{a,b,c}|^2$ : following the gain reconfiguration at  $t = 60$  ms, the system stalls at an intermediate state  $\{0.47 - 0.64i, 1, 1\}$  rather than converging to the intended target after transition. While the energy in resonators  $b$  and  $c$  (yellow and cyan curves) do increase and resonator  $a$  (blue curve) decreases after the switch, the final energy contrast falls far short of the design goal: resonator  $a$  retains significant amplitude instead of being fully suppressed. This trapping stems from a symmetry mismatch: eigenmode  $\psi_1$  (before transition) has resonators  $b$  and  $c$  oscillating in-phase, while target  $\psi'_1$  requires them out-of-phase. The parity-symmetric gain  $(0, g_0, g_0)$  across resonators  $b$  and  $c$  thus cannot induce the target mode transition. While in practice, we would expect any noise or impaction in the system in breaking such parity symmetry will ultimately collapse into the target mode, here we can accelerate this with transient perturbations  $g'_b$  shown in Fig. 4(b)(iii), which purposely breaks the  $b$ - $c$  symmetry at transition points. Fig. 4(d) demonstrates the result: with

$g'_b$  applied, the system successfully converges to  $\psi'_1$  by  $t = 100$  ms, achieving complete energy redistribution with resonator  $a$  suppressed and  $b, c$  equally enhanced but out-of-phase.

This demonstrates how temporal modulation controls not only eigenmode selection but also transition dynamics. Here, small perturbations dramatically enhance convergence rates by breaking symmetry constraints that otherwise trap the system in metastable states. The framework thus provides both target selection through spatial profiles and convergence acceleration through temporal perturbations.

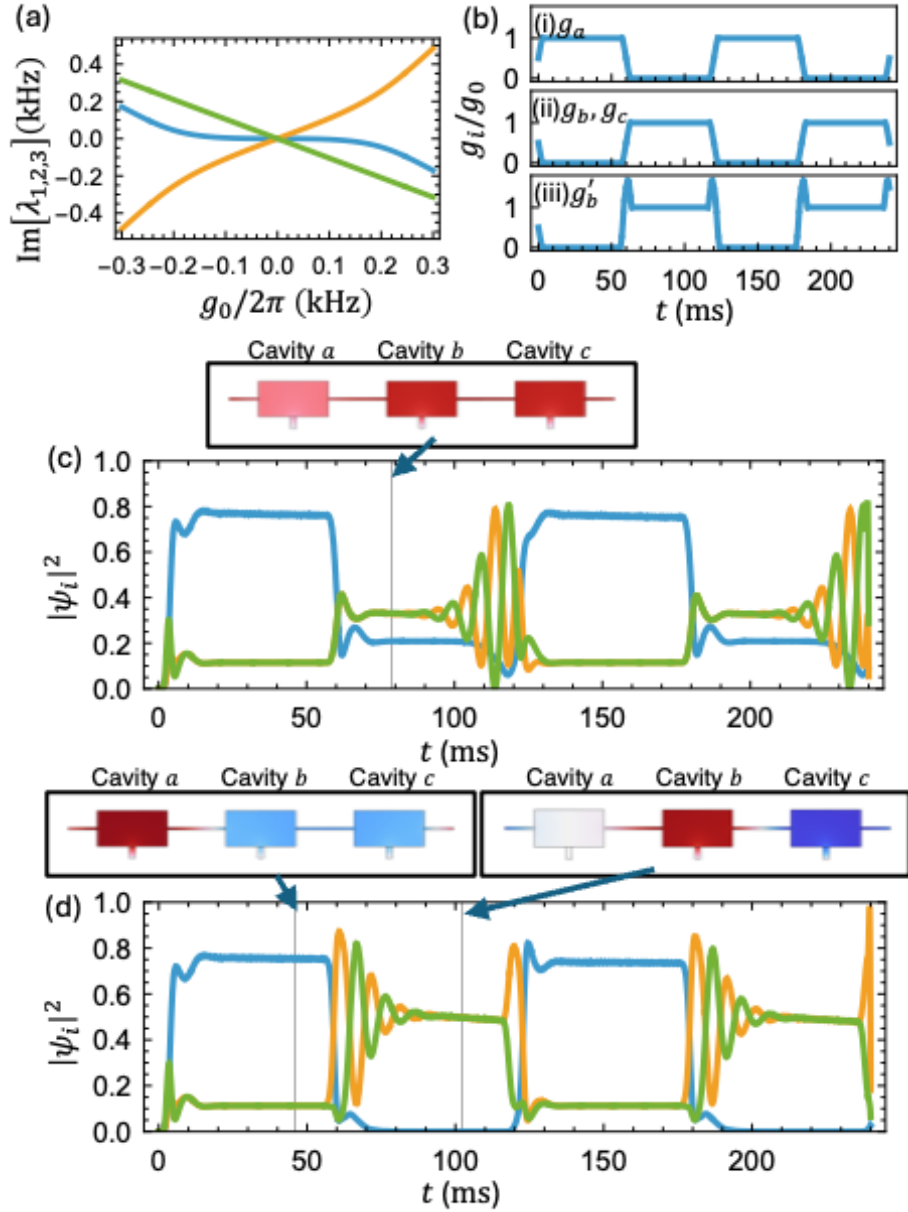


Figure 4 (a) Imaginary part of eigenvalues of the effective Hamiltonian  $H_{\text{eff}}$  for single-cavity amplification:  $(g_a, g_b, g_c) = (g_0, 0, 0)$ . (b) Modulation schemes for gain-loss parameters  $g_a, g_b, g_c$  comparing two cases: (i,ii) symmetric modulation without perturbation where  $g_b =$

$g_c$  throughout, and (iii) asymmetric modulation with perturbation  $g'_b$  at transition points. The modulation alternates between concentrating energy in cavity  $a$  using  $(g_a, g_b, g_c) = (g_0, 0, 0)$  during  $t \in \{0, 60\}, \{120, 180\}$  ms, and redistributing energy to cavities  $b$  and  $c$  using  $(g_a, g_b, g_c) = (0, g_0, g_0)$  during  $t \in \{60, 120\}, \{180, 240\}$  ms. (c) Simulation without perturbation: energy successfully concentrates in cavity  $a$  during the first 60 ms (matching Fig. 3(c)) but fails to redistribute to cavities  $b$  and  $c$  during  $60 < t < 120$  ms, unable to reach the target eigenmode  $\psi'_1 = \{0, 1, -1\}$ . (d) Simulation with perturbation  $g'_b$  showing that the symmetry-breaking perturbation enables successful energy redistribution, with the system converging to  $\psi'_1$  at  $t \cong 100$  ms.

We have demonstrated that a  $\mathcal{PT}$ -symmetric system with cross-site nonlinearity enables precise control of wave amplitudes while maintaining energy conservation across the system. Our theoretical framework reveals how fixed-point solutions correspond to eigenvectors of an effective Hamiltonian, with exceptional points separating  $\mathcal{PT}$ -broken phases (exhibiting stable equilibrium) from  $\mathcal{PT}$ -symmetric phases (displaying oscillatory behavior). The extension to three-cavity systems showcases enhanced control capabilities through periodic modulation of gain-loss parameters, enabling programmable energy distribution among cavities and accelerating mode transitions via temporal perturbations. Simulation validation using Helmholtz resonators confirms the feasibility of this approach, opening new avenues for acoustic wave manipulation in applications ranging from noise control to acoustic information processing, while providing fundamental insights into the interplay between nonlinearity,  $\mathcal{PT}$  symmetry, and wave dynamics in coupled resonant systems.

## Acknowledgments

The work is supported from the EPSRC via the META4D Programme Grant (No. EP/Y015673/1).

## References

- 1 N. Yu, P. Genevet, M. A. Kats, F. Aieta, J.-P. Tetienne, F. Capasso, and Z. Gaburro, Light Propagation with Phase Discontinuities: Generalized Laws of Reflection and Refraction, *Science* **334**, 333 (2011).
- 2 G. Zheng, H. Mühlenbernd, M. Kenney, G. Li, T. Zentgraf and S. Zhang, Metasurface Holograms Reaching 80% Efficiency, *Nat. Nanotechnol.* **10**, 4 (2015).
- 3 C. M. Soukoulis, S. Linden, and M Wegener, Negative refractive index at optical wavelengths, *Science* **315**, 47-49(2007).
- 4 J. B. Pendry, Negative refraction makes a perfect lens, *Phys. Rev. Lett.* **85**, 3966 (2000).
- 5 S. Wang, P. C. Wu, V.-C. Su, Y.-C. Lai, M.-K. Chen, H. Y. Kuo, B. H. Chen, Y. H. Chen, T.-T. Huang, J.-H. Wang, R.-M. Lin, C.-H. Kuan, T. Li, Z. Wang, S. Zhu, and D. P. Tsai, A broadband achromatic metalens in the visible, *Nat. Nanotechnol.* **13**, 227 (2018).

- 6 X. Ni, Z. J. Wong, M. Mrejen, Y. Wang, and X. Zhang, An ultrathin invisibility skin cloak for visible light, *Science* **349**, 1310 (2015).
- 7 S. Zhang, D. A. Genov, Y. Wang, M. Liu, and X. Zhang, Plasmon-induced transparency in metamaterials, *Phys. Rev. Lett.* **101**, 047401 (2008).
- 8 Q. Li, Z. Zhang, L. Qi, Q. Liao, Z. Kang, and Y. Zhang, Toward the application of high frequency electromagnetic wave absorption by carbon nanostructures, *Adv. Sci.* **6** (8), 1801057 (2019).
- 9 J. Zhou, S. Liu, H. Qian, Y. Li, H. Luo, S. Wen, Z. Zhou, G. Guo, B. Shi, and Z. Liu, Metasurface enabled quantum edge detection, *Sci. Adv.* **6**, eabc4385 (2020).
- 10 Y. Li, B. Liang, Z.-m. Gu, X.-y. Zou, and J.-C. Cheng, Reflected wavefront manipulation based on ultrathin planar acoustic metasurfaces, *Sci. Rep.* **3**, 2546 (2013).
- 11 J. Li, and C. T. Chan, Double-negative acoustic metamaterial, *Phys. Rev. E* **70**, 055602(R) (2004).
- 12 L. Wu, X. Qiu, and Y. Guo, A simplified adaptive feedback active noise control system, *Applied Acoustics* **81**, 40 (2014).
- 13 B.-I. Popa, Y. Zhai, and H.-S. Kwon, Broadband sound barriers with bianisotropic metasurfaces, *Nat. Commun.* **9**, 5299 (2018).
- 14 Y. Xie, W. Wang, H. Chen, A. Konneker, B.-I. Popa, and S. A. Cummer, Wavefront modulation and subwavelength diffractive acoustics with an acoustic metasurface, *Nat. Commun.* **5**, 5553 (2014).
- 15 M. Yan, J. Lu, F. Li, W. Deng, X. Huang, J. Ma, and Z. Liu, On-chip valley topological materials for elastic wave manipulation, *Nat. Mater.* **17**, 993 (2018).
- 16 R. Zhu, X. N. Liu, G. K. Hu, C. T. Sun, and G. L. Huang, A chiral elastic metamaterial beam for broadband vibration suppression, *J. Sound Vib.* **333**, 2759 (2014).
- 17 J. B. Pendry, D. Schurig, and D. R. Smith, Controlling electromagnetic fields, *Science* **312**, 1780 (2006).
- 18 D. Schurig, J. J. Mock, B. J. Justice, S. A. Cummer, J. B. Pendry, A. F. Starr, and D. R. Smith, Metamaterial electromagnetic cloak at microwave frequencies, *Science* **314**, 977 (2006).
- 19 S. A. Cummer, and D. Schurig, One path to acoustic cloaking. *New J. Phys.* **9**, 45 (2007).
- 20 Y. Ra'Di, and A. Grbic, Magnet-free nonreciprocal bianisotropic metasurfaces, *Phys. Rev. B* **94**, 195432 (2016).
- 21 Y. Zhai, H. S. Kwon, and B. I. Popa Active Willis metamaterials for ultracompact nonreciprocal linear acoustic devices, *Phys. Rev. B* **99**, 220301 (2019).
- 22 K. G. Makris, Z. H. Musslimani, D. N. Christodoulides, and S. Rotter, Constant-intensity waves and their modulation instability in non-Hermitian potentials, *Nat. commun.* **6**, 7257 (2015).
- 23 E. Rivet, A. Brandstötter, K. G. Makris, H. Lissek, S. Rotter, and R. Fleury, Constant-pressure sound waves in non-Hermitian disordered media, *Nat. Phys.* **14**, 942 (2018).
- 24 S. Yu, X. Piao, and N. Park, Bohmian Photonics for Independent Control of the Phase and Amplitude of Waves, *Phys. Rev. Lett.* **120**, 193902 (2018).
- 25 C. M. Bender, and S. Böttcher, Real Spectra in Non-Hermitian Hamiltonians Having  $\mathcal{PT}$  Symmetry, *Phys. Rev. Lett.* **80**, 5243 (1998).
- 26 R. El-Ganainy, K. G. Makris, M. Khajavikhan, Z. H. Musslimani, S. Rotter, and D. N. Christodoulides, Non-Hermitian physics and PT symmetry, *Nat. Phys.* **14**, 11 (2018).
- 27 L. Feng, Z. J. Wong, R.-M. Ma, Y. Wang, and X. Zhang, Single-mode laser by parity-time symmetry breaking, *Science* **346**, 972 (2014).
- 28 H. Hodaei, M.-A. Miri, A. U. Hassan, W. E. Hayenga, M. Heinrich, D. N. Christodoulides, and M. Khajavikhan, Single mode lasing in transversely multi-moded PT-symmetric microring resonators, *Laser Photonics Rev.* **10**, 494 (2016).
- 29 M.H. Teimourpour, M. Khajavikhan, D.N. Christodoulides, and R. El-Ganainy, Robustness and mode selectivity in parity-time (PT) symmetric lasers, *Sci. Rep.* **7**, 10756 (2017).

- 30 Q. Zhong, S.K. Ozdemir, A. Einfeld, A. Metelmann, and R. El-Ganainy, Exceptional-Point-Based Optical Amplifiers, *Phys. Rev. Appl.* **13**, 014070 (2020).
- 31 X. Wen, H. K. Yip, C. Cho, J. Li, and N. Park, Acoustic Amplifying Diode Using Nonreciprocal Willis Coupling, *Phys. Rev. Lett.* **130**, 176101 (2023).
- 32 S. Xiao, J. Gear, S. Rotter, and J. Li, Effective PT-symmetric metasurfaces for subwavelength amplified sensing, *New J. Phys.* **18**, 085004 (2016).
- 33 M. Farhat, M. Yang, Z. Ye, and P.-Y. Chen, PT-Symmetric Absorber-Laser Enables Electromagnetic Sensors with Unprecedented Sensitivity, *ACS Photonics* **7**, 2080 (2020).
- 34 X. Guo, Y. Ding, Y. Duan, and X. Ni, Nonreciprocal metasurface with space-time phase modulation. *Light:Sci. Appl.* **8**, 123 (2019).
- 35 S. Taravati, Giant linear nonreciprocity, zero reflection, and zero band gap in equilibrated space-time-varying media, *Phys. Rev. Appl.* **9**, 064012 (2018).
- 36 N. A. Estep, D. L. Sounas, J. Soric, and A. Alù, Magnetic-free non-reciprocity and isolation based on parametrically modulated coupled-resonator loops, *Nat. Phys.* **10**, 923 (2014).
- 37 R. Tirole, S. Vezzoli, D. Saxena, S. Yang, T. V. Raziman, E. Galiffi, S. A. Maier, J. B. Pendry, and R. Sapienza, Second harmonic generation at a time-varying interface. *Nat. Commun.* **15**, 7752 (2024).
- 38 H. Moussa, G. Xu, S. Yin, E. Galiffi, Y. Ra'di, and A. Alù, Observation of temporal reflection and broadband frequency translation at photonic time interfaces, *Nat. Phys.* **19**, 863 (2023).
- 39 R. Tirole, S. Vezzoli, E. Galiffi, I. Robertson, D. Maurice, B. Tilmann, S. A. Maier, J. B. Pendry, and R. Sapienza, Double-slit time diffraction at optical frequencies, *Nat. Phys.* **19**, 999 (2023).
- 40 E. Galiffi, P. A. Huidobro, and J. B. Pendry, Broadband nonreciprocal amplification in luminal metamaterials, *Phys. Rev. Lett.* **123**, 206101 (2019).
- 41 J. B. Pendry, E. Galiffi, and P. A. Huidobro, Gain in time-dependent media—a new mechanism, *J. Opt. Soc. Am. B* **38**, 3360 (2021).
- 42 Q. Yang, H. Hu, X. Li, and Y. Luo, Cascaded parametric amplification based on spatiotemporal modulations, *Photonics Res.* **11**, B125 (2023).
- 43 T. T. Koutserimpas, A. Alù, and R. Fleury, Parametric amplification and bidirectional invisibility in  $\mathcal{PT}$ -symmetric time-Floquet systems, *Phys. Rev. A* **97**, 013839 (2018)
- 44 A. Guo, G. J. Salamo, D. Duchesne, R. Morandotti, M. Volatier-Ravat, V. Aimez, G. A. Siviloglou, and D. N. Christodoulides, Observation of  $\mathcal{PT}$ -Symmetry Breaking in Complex Optical Potentials, *Phys. Rev. Lett.* **103**, 093902 (2009)
- 45 L. Ge, and R. El-Ganainy, Nonlinear modal interactions in parity-time (PT) symmetric lasers, *Sci. Rep.* **6**, 24889 (2016).
- 46 C. Shen, X. Zhu, J. Li, and S. A. Cummer, Nonreciprocal acoustic transmission in space-time modulated coupled resonators, *Phys. Rev. B* **100**, 054302 (2019).
- 47 M. Rupin, G. Lerosey, J. d. Rosny, and F. Lemoult, Mimicking the cochlea with an active acoustic metamaterial, *New J. Phys.* **21**, 093012 (2019).